Atmospheric
Measurement
Techniques
Discussions

Retrieval and validation of METOP/IASI methane

Evelyn De Wachter[1], Nicolas Kumps[1], Ann Carine Vandaele[1], Bavo Langerock[1], and Martine De Mazière[1]

[1]Royal Belgian Institute for Space Aeronomy (BIRA-IASB), 1180 Brussels, Belgium

Correspondence to: Evelyn De Wachter (evelyn.dewachter@aeronomie.be)

Abstract. A new global IASI methane product developed at the Royal Belgian Institute for Space Aeronomy (BIRA-IASB) is presented. The retrievals are performed with the ASIMUT-ALVL software based on the Optimal Estimation Method (OEM). This paper gives an overview of the forward model and retrieval concept. The usefullness of reconstructed Principal Component Compressed (PCC) radiances is highlighted. The retrieval uncertainty of the CH_4 profiles is less than 4% below 100 hPa

5 ($\sim$16 km). The information content study carried out in this paper shows that most IASI pixels contain between 0.9 and 1.6 independent pieces of information about the vertical distribution of CH_4, with a good sensitivity in the mid to upper troposphere. An extended validation with ground-based CH_4 observations at 10 locations was carried out. IASI CH_4 partial columns are found to correlate well with the ground-based data for 7 out of the 10 Fourier Transform Infrared (FTIR) stations with correlation coefficients between 0.71 and 0.96. Mean differences between IASI and FTIR CH_4 range between -1.93 and

10 4.40% and are within the systematic uncertainty. For 7 out of the 10 stations absolute differences are less than 1%. The standard deviation of the difference lies between 1.40 and 3.99% for all the stations.

1 Introduction

There is now a widespread scientific consensus on the profound influence of human activity on the global climatic system, particularly through increased emissions of greenhouse gases like CO_2 and CH_4 since the pre-industrial era (Jardine et al.,

15 2009). Although CH_4 is roughly 200 times less abundant in the atmosphere than CO_2, it is a more potent greenhouse gas. The comparative impact of CH_4 on climate change is more than 86 times greater than CO_2 over a 20-year period (Myhre et al. , 2013). Identified CH_4 emission sources are either of biogenic, pyrogenic or thermogenic origin. CH_4 emissions of biogenic origin are related to anaerobic decomposition; a collection of processes by which microorganisms break down organic matter in the absence of oxygen. Examples are natural wetlands, oxygen-poor freshwater reservoirs, digestive systems of

20 ruminants, rice paddies and waste treatment (Kirschke et al., 2013). Pyrogenic CH_4 is produced by the incomplete combustion of biomass and soil carbon during wildfires and of biofuels and fossil fuels. Thermogenic sources comprise the exploitation of oil, natural gas and coal and the natural degassing from the subsurface such as terrestrial seeps, marine seeps and mud volcanoes (Kirschke et al., 2013). The primary sink for atmospheric CH_4 is oxidation by hydroxyl radicals (OH), mostly in the troposphere, which accounts for about 90% of the global CH_4 sink (Kirschke et al., 2013). In addition, CH_4 is depleted

25 at the surface by consumption by soil bacteria and by its reaction with chlorine radicals in the marine boundary layer. These processes amount to a lifetime of atmospheric CH_4 of $\sim$9 years.

Atmospheric
Measurement
Techniques
Discussions

Since 2014, atmospheric CH_4 concentrations are rising faster than at any time in the past two decades and are now approaching the most greenhouse gas-intensive scenarios (Saunois et al., 2016). Its concentration has more than doubled since the pre-industrial period, reaching a new high of 1845 ± 2 ppb in 2015, an increase of 11 ppb with respect to the previous year, as shown by the latest analysis of observations from the World Meteorological Organization (WMO) Global Atmosphere Watch (GAW)

5 Programme (WMO News Bulletin , 2016). CH_4 is a challenging atmospheric component to study as its non-monotonous changes in the last decades and its interannual variability remain not fully understood (Nisbet et al. , 2014). The mean annual growth rate of CH_4 decreased from 14 ppb/yr in 1984 to near zero in 1999 (Dlugokencky et al., 2003). From 1999 to 2006, globally averaged CH_4 was relatively constant but atmospheric methane concentrations started rising again in 2007 with a global average growth of $\sim$6 ppb/year (Nisbet et al. , 2014). Latest analysis by Saunois et al. (2016) suggests that the cause

10 of the atmospheric growth trend of the past decade is predominantly biogenic - most likely from agriculture - with smaller contributions from fossil fuel use and possibly wetlands.

Our current understanding of the natural and anthropogenic emissions of CH_4 is insufficient. Although the global OH sink of CH_4 and the sum of CH_4 sources is relatively well known, there are still large uncertainties about each of the individual sources of CH_4. However, due to its relatively short lifetime, it is now recognized that one of the most efficient methods to mitigate

15 warming due to greenhouse gases on decadal time frames is to cut CH_4 emissions (Shindell et al. , 2012). Global monitoring of CH_4 is therefore essential to increase our knowledge on how the different sources and sinks influence the atmospheric abundance of methane.

Atmospheric CH_4 has been measured continuously from space since 2003. Jacob et al. (2016) gives an extensive overview of past and future satellite missions dedicated to detect methane. Atmospheric CH_4 is detectable by its absorption of radiation

20 in the shortwave infrared (SWIR) and thermal infrared (TIR). SWIR instruments, such as SCIAMACHY (Frankenberg et al., 2006), TANSO-FTS (Kuze et al. , 2016) and the soon to be launched TROPOMI instrument (Hu et al., 2016), measure the solar radiation backscattered by the Earth and the atmosphere, and give a total atmospheric column of CH_4 with near uniform sensitivity in the troposphere (Jacob et al., 2016). TIR instruments measure the thermal radiation emitted by the Earth and the atmosphere, and operate in a nadir, limb or solar occultation observing mode. Limb and solar occultation detect CH_4

25 vertical profiles in the stratosphere and upper troposphere (Jacob et al., 2016). TIR nadir measurements provide integrated CH_4 columns in the middle to upper troposphere and allow day and nighttime concentrations, over land and sea. Examples are the AIRS instrument onboard the NASA Aqua satellite which has been providing global methane observations since 2002 (Xiong et al., 2008), TES which was operational from 2004 to 2011 (Worden et al., 2012), and IASI, launched onboard METOP-A in October 2006 and on METOP-B in September 2012 (Razavi et al. , 2009; Crevoisier et al., 2009; Xiong et al., 2013). With the

30 launch of MERLIN foreseen in 2021, for the first time, active measurements will be made from space with an IPDA (Integrated Path Differential Absorption) LIDAR (Light Detecting And Ranging), which will provide atmospheric methane columns with high precision and unprecedented accuracy on a global scale (Pierangelo et al. , 2016).

In this paper, we present a new CH_4 product retrieved from IASI radiances with the ASIMUT-ALVL software developed at BIRA-IASB. This product complements the BIRA-IASB height-resolved IASI aerosol dust product (Vandenbussche et al.,

35 2013). Sect. 2 introduces the IASI mission. In Sect. 3 we describe the IASI CH_4 radiative transfer and the retrieval setup, and

the use of the Principal Component Compressed IASI spectra is addressed. The information content of the IASI CH_4 product is presented in Sect. 4. In addition, global distributions are shown and retrieval processing details are briefly discussed. In Sect. 5 the IASI CH_4 product is compared to ground-based measurements, providing an quality assessment of the retrieved BIRA-IASB CH_4 columns. The final section summarizes the main results of this work.

2 IASI

The Infrared Atmospheric Sounding Interferometer (IASI) onboard MetOp, is a thermal cross-nadir scanning infrared sounder. Launched in October 2006, it is the first in a successive series of three, together programmed to provide measurements for a period of 15 years. The second instrument onboard MetOp-B was launched in September 2012 and the launch of MetOp-C is scheduled for October 2018.

IASI is a Fourier Transform Infrared (FTIR) spectrometer which measures the TIR radiation emitted by the Earth and the atmosphere. With a wide swath width of 2 x 1100 km it provides near-global coverage twice a day, with a local overpass time at ~9:30 AM and PM. It has an instantaneous field of view (FOV) at nadir with a spatial resolution of 50 km x 50 km, composed of 2 x 2 circular pixels, each corresponding to a 12 km diameter footprint on the ground at nadir (Clerbaux et al., 2009). IASI has four spectral bands in the spectral range from 645 to 2760 cm^{-1} (3.62 to 15.5 µm), with an apodized spectral resolution of 0.5 cm^{-1} and spectral sampling of 0.25 cm^{-1}.

Designed to provide highly accurate temperature and humidity profiles for numerical weather predictions, the IASI mission allows simultaneous global observations of the air composition with an excellent spatial resolution. From the atmospheric spectra recorded by the instrument, concentrations of several trace gases can be monitored, enhanced levels of pollution can be detected, and particle types can be determined to some extent. On the longer term the continuity of the program is ensured with the IASI-NG mission that will extend the IASI observation for 15-20 more years (Clerbaux et al., 2016).

3 The IASI CH_4 retrieval method

The IASI CH_4 profiles are retrieved with the ASIMUT-ALVL software developed at BIRA-IASB (Vandaele et al., 2006). ASIMUT-ALVL is a modular software for radiative transfer (RT) calculations and inversions in planetary atmospheres. The code has been developed with the objective to be as general as possible, accepting different instrument types and different geometries. ASIMUT-ALVL has been coupled to the SPHER/TMATRIX (Mishchenko and Travis , 1998) and LIDORT (Spurr , 2006) codes to include the complete treatment of the scattering effects into the RT calculations. It has a specific interface dealing with the IASI instrument characteristics and IASI input information and is also used for the IASI aerosol dust retrievals (Vandenbussche et al., 2013). The RT simulations are performed with the ASIMUT-ALVL RT code for the IASI CH_4 data product while the LIDORT RT code is used for the IASI aerosol dust retrievals in order to include all scattering effects due to aerosols. Both IASI retrieval products use the same retrieval module, based on the formalism of the Optimal Estimation Method (OEM) (Rodgers, 2000).

Atmospheric
Measurement
Techniques
Discussions

Initially developed for Earth observation missions, ASIMUT-ALVL has also been adapted for planetary atmospheres, in particular those of Venus (Vandaele et al., 2008) and Mars (Drummond et al., 2011) and is now the reference code for the NOMAD instrument on-board ExoMars TGO (Robert et al., 2016).

3.1 Forward model

5 The ASIMUT-ALVL RT module simulates atmospheric transmittances and radiances for cases under local thermodynamical equilibrium and where scattering can be neglected. A detailed description of the radiative transfer model is given in Vandaele et al. (2006). The spectral range considered for the CH_4 retrieval is the 1210-1290 cm^{-1} range covering part of the $\nu 4$ spectral band. EUMETSAT IASI L2 temperature and water vapour profiles are used as input for the radiative transfer calculations. The spectroscopic parameters for CH_4, N_2O and other species are taken from the HITRAN 2012 database (Rothman et al., 2013).

10 The IASI Instrument Line Shape (ILS) is characterized by a Gaussian function with a 0.5 cm^{-1} FWHM. Frequency dependent emissivity maps are provided by Zhou et al. (2011). Fig. 1 shows an example of measured and simulated radiances in the 1210-1290 cm^{-1} spectral range and its residual (difference between measured and simulated radiances). We have a negligible bias and a 1-σ standard deviation comparable to the radiometric noise of $2x10^{-8}$ W/(cm^2 sr cm^{-1}) (see Sect. 3.2). Certain spectral ranges in the considered spectral band are not well simulated by the radiative transfer model, leading to outliers in the

15 residuals with absolute differences larger than $5x10^{-8}$ W/(cm^2 sr cm^{-1}), for example at 1246 cm^{-1} and 1252 cm^{-1}. These spectral ranges are masked in the retrieval set-up, i.e. the radiometric noise is set to zero at these spectral points, so that no information is lost.

Only IASI L1C spectra with a cloud fraction < 10% based on the EUMETSAT IASI L2 fractional cloud cover product are processed.

20 ### 3.2 Retrieval and error characterization

The ASIMUT retrieval module is based on the OEM (Rodgers, 2000) where the Jacobians are calculated analytically. The characteristics of the IASI retrieval are summarized in Table 6. The state vector includes the skin temperature (T_{skin}), 23-level CH_4, N_2O and H_2O profiles and a CO_2 total column. The T_{skin} a priori is taken from the EUMETSAT IASI L2 T_{skin} product. The a priori profiles x_a and covariance matrices S_a for CH_4 and N_2O are based on a climatology from the WACCM model. The

25 H_2O a priori uncertainty covariance matrix is characterised by an uncertainty covariance matrix with a 10% standard deviation on the diagonal and an exponential decaying correlation width of 6 km. The EUMETSAT IASI L2 water vapour profile is used as the H_2O a priori profile x_a. The interfering species HNO_3 and O_3 are included in the RT calculations, its a priori values are provided by the WACCM model.

A diagonal measurement uncertainty covariance S_e is taken, with the radiometric noise set to $2x10^{-8}$ W/(cm^2 sr cm^{-1}). This

30 value is conservative, about a factor 5 higher than the estimated radiometric noise in this spectral region of $4x10^{-9}$ W/(cm^2 sr cm^{-1}) (Clerbaux et al., 2009). It includes not only the measurement uncertainty, but also the uncertainties in the temperature and water vapor profile, the spectroscopic parameters and surface emissivity (De Wachter et al., 2012).

Fig. 2 presents the CH_4 a priori profile (pink) and retrieved CH_4 profile (blue) in volume mixing ratio (vmr) for a pixel at 27°N.

The horizontal bars represent the retrieval uncertainty. The averaging kernel (AK) is given in the middle figure. It shows that the sensitivity of the IASI CH_4 product lies in the 800-100 hPa ($\sim$2-16 km) range.

The right plot of Fig. 2 diplays the vertical profiles of the retrieval uncertainties together with the CH_4 a priori variability (black line). The square root of the diagonal elements of the uncertainty is plotted. The CH_4 a priori variability is calculated from the square root of the diagonal of the a priori uncertainty covariance matrix. The retrieval is quite constrained with of an a priori variability of a few percent at the surface going up to 7-8% at 20 km. Following Rodgers (2000) the error sources contributing to the total retrieval uncertainty are 1) the smoothing error, which accounts for the vertical resolution of the retrieved CH_4, 2) the error due to uncertainties in forward model parameters such as spectroscopy, the temperature profile, surface emissivity and 3) the IASI measurement uncertainty. For IASI the forward model uncertainties are included in the measurement uncertainty. As we can see from Fig. 2, the dominant source of uncertainty is the smoothing uncertainty. The total retrieval uncertainty declines from 3% at the su rface to $\sim$2% between 800 and 200 hPa, the altitude range of maximum sensitivity. Above 200 hPa the total retrieval uncertainty increases rapidly up to $\sim$4% at 100 hPa and $\sim$6% at 60 hPa.

3.3 Retrievals with PCC L1C data

The CH_4 profiles are retrieved from IASI radiances recomposed from the EUMETSAT Principal Component Compressed (PCC) L1C dataset (Hultberg , 2009). The use of PCC data allows both noise filtering and a large reduction in data volume compared to the use of raw radiances. Our main motivation is the large reduction in data storage. One year of the original IASI L1C (BUFR format) data amounts to 10 Tb which is reduced to 1 Tb/year for the PCC data. Fig. 3 shows the raw and PCC radiances for a random pixel in the CH_4 $\nu 4$ spectral band. Differences between raw radiances and PCC radiances lie in the IASI radiometric noise level (4×10^{-9} W/(m^2 sr m^{-1})) as given by the IASI radiometric noise figure from Clerbaux et al. (2009). This is a factor 5 lower than the conservative radiometric noise level of 2×10^{-8} W/(m^2 sr m^{-1}) used in the CH_4 retrieval (see Sect. 3.1). Fig. 4 compares the CH_4 concentrations retrieved with the PCC L1C data with those retrieved with the raw radiances for March 2011 and September 2013 for daytime retrievals between 60°S and 70°N. We find an excellent correlation (R=1) between the retrieved concentrations and negligibles biases of 0.0026% and 0.025% with a 1-σ standard deviation of $\leqslant$0.12%. With these results we are confident to use the PCC-reconstructed radiances.

4 The BIRA-IASB IASI CH_4 product

4.1 Information content

For correct interpretation of the data one needs to consider the vertical sensitivity of the retrieved CH_4 profile. This information is contained in the averaging kernel (AK), which is provided with each retrieved CH_4 profile. The peak of each AK gives the altitude of maximum sensitivity. Its full width at half maximum can be interpreted as the vertical resolution of the retrieval. Averaging kernels are variable, as can be seen from Fig. 5. Given is the CH_4 AK for 3 pixels in March 2013 at 3 different geographical locations; at northern mid-latitudes (55 °N), in the tropics (4 °N) and at southern mid-latitudes (47 °S). In the

Atmospheric
Measurement
Techniques
Discussions

Open Access

EGU

tropics, the CH_4 sensitivity lies in the 850-100 hPa (∼1.5-16 km) range, at mid-latitudes, in the 700-200 hPa (∼3-12 km) range. For the 3 geographical locations, the sensitivity is reduced in the boundary layer, which is typical for thermal infrared sounders. In each figure the Degree of Freedom for Signal (DOFS) is given, which is an estimate of the number of independent pieces of information contained in the measurement. It is the trace of the AK. One independent piece of information (1.01 < DOFS

5   < 1.47) is deduced for the 3 geographical locations. Maps of the CH_4 DOFS for February and August 2013 are presented in Fig. 6. DOFS values for daytime retrievals are shown in the 2 lefthand figures, DOFS values for nighttime retrievals are shown in the 2 righthand figures. For both seasons and day- or nighttime retrievals we typically have DOFS values in the tropics around 1.4. For the Northern Hemisphere (NH), at mid-latitudes, we see higher DOFS values in August (NH summer) than in February (NH winter). In February values can become less than 1 for latitudes > 40°N. The variability of the AK (and hence

10 the DOFS) is dependent on the thermal contrast, which exhibits significant geographical, seasonal, and diurnal variability. The retrieval sensitivity is favourable, and hence the DOFS is high, when thermal contrast is high. In general the thermal contrast or the DOFS is higher during the day, over land, and over dry, sparsely vegetated regions (Clerbaux et al., 2009). This pattern is visible in Fig. 6, where DOFS values are generally higher for daytime retrievals compared to the nighttime retrievals, and where high DOFS values are found for the daytime observations at desert regions of Africa and Australia. The DOFS for different

15 latitudinal bands for February and August 2013 is presented in Fig. 7. DOFS values for daytime retrievals are provided in the 2 lefthand figures, DOFS values for nighttime retrievals are shown in the 2 righthand figures. This figure confirms that DOFS values in the tropics are typically around 1.4. For August (NH summer), on the global scale, the DOFS values for daytime retrievals range between 1 and 1.8 (between 0.9 and 1.6 for nighttime retrievals). For February (NH winter), values range between 0.4 and 1.7 (between 0.4 and 1.6 for nighttime retrievals), when values can become less than 1 for latitudes > 40°N.

20 So overall one independent piece of information is retrieved with a good sensitivity in the mid to upper troposphere.

4.2   Global distributions

Monthly mean global daytime distributions for the year 2013 are presented in Fig. 8. IASI CH_4 partial columns between 4 and 17 km between 60°S and 70°N are shown for the IASI morning overpass. CH_4 concentrations are averaged over the four, 2 x 2 circular IASI pixels, which are measured simultaneously (see Sect. 2) and binned on a 1° x 1° grid. Areas with missing data

25 correspond to areas which were identified as cloudy by the EUMETSAT IASI L2 fractional cloud cover product, or correspond to areas where not all of the 4 simultaneously measured pixels converged in the retrieval.

We see a latitudinal gradient with higher concentrations in the Northern Hemisphere (NH) than in the Southern Hemisphere (SH), which is consistent with the fact that most of the methane sources are located in the Northern Hemisphere. In the NH, higher CH_4 concentrations are found during boreal summer than during boreal winter. This summer increase of mid to upper

30 tropospheric CH_4 has also been observed by AIRS (Xiong et al., 2010). van Weele et al. (2011) examined the CH_4 variability in the upper troposphere and lower stratosphere between ∼6-25 km using aircraft observations and the TM5-chem-v3.0 chemistry transport model (Krol et al., 2005; Huijnen et al. , 2010). They also found higher CH_4 mixing ratios at the 500 hPa level (∼6 km) at high latitudes during boreal summer compared to winter concentrations and attributed the winter minimum to enhanced downward transport from the stratosphere.

Methane observed in the boundary layer by surface stations from the NOAA network displays a reversed seasonal cycle in the NH (Dlugokencky et al., 2009). These results demonstrate the added value of thermal infrared CH_4 measurements which have a sensitivity at higher altitudes.

4.3 Retrieval output and processing

5   The BIRA-IASB IASI CH_4 product is delivered in HDF5 format. Daily daytime and nighttime observations are provided in separate files. The HDF files contain CH_4 profiles, the retrieval uncertainty, the CH_4 a priori profiles and averaging kernels. BIRA-IASB entered Phase 2 of the Climate Change Initiative-Greenhouse Gas (CCI-GHG) project (Buchwitz et al., 2015) and a dataset has been generated for the years 2011-2014, contributing to Climate Research Data Package No.4 (CRDP#4). These retrievals were performed between 60°S and 70°N and can be downloaded from http://iasi.aeronomie.be/. Data is processed

10 on a High Performance computing system (HPC) with 2 x 55 nodes of 24 Central Processing Units (CPUs) where the user obeys a quota-based use. One day of IASI CH_4 data (for the 60°S and 70°N region) is processed in 48 hours on 1 node with 24 CPUs.

5   Validation

Ground-based data was collected from 10 FTIR stations from the Network for the Detection of Atmospheric Composition

15 Change (NDACC). The stations chosen are operated on a quasi-continuous basis and deliver CH_4 vertical profiles. Certain stations provide limited observations since they only recently entered the NDACC network or since they only make campaign measurements. We therefore excluded stations with less than 200 collocations due to insufficient collocation points for a statistically significant comparison. NDACC FTIR CH_4 profiles have good sensitivity in the troposphere and stratosphere with 2 to 3 independent pieces of information. Note, the NDACC CH_4 retrieval is not fully harmonized yet for all the NDACC

20 stations. This work is ongoing as part of the Horizon 2020 Gap Analysis for Integrated Atmospheric ECV CLImate Monitoring (GAIA-CLIM) project (http://www.gaia-clim.eu/).

We performed a detailed comparison between IASI and NDACC CH_4 partial columns between 4 and 17 km at these 10 NDACC stations for the period 2011 to 2014. Since the two retrievals have been computed with a different a priori, the NDACC retrieved profiles are adjusted for the comparison. Following Rodgers and Connor (2003) (equation 10), the term

25 $(\mathbf{A_{NDACC}} - \mathbf{I}) \cdot (\mathbf{x_{a,NDACC}} - \mathbf{x_{a,IASI}})$ is added to each NDACC retrieval to adjust for the different a priori profile used in the IASI retrieval. Here $\mathbf{A_{NDACC}}$ is the NDACC averaging kernel, $\mathbf{I}$ the unity matrix, $\mathbf{x_{a,NDACC}}$ the NDACC CH_4 a priori profile and $\mathbf{x_{a,IASI}}$ the IASI CH_4 a priori profile.

In addition, to account for the different resolution between the IASI and the higher resolved NDACC FTIR profiles, a smoothing is applied to the (a priori adjusted) NDACC profile $\mathbf{x_{NDACC}}$ by the IASI averaging kernel:

30 $$\mathbf{\hat{x}_{NDACC}} = \mathbf{x_{a,IASI}} + \mathbf{A_{IASI}} \cdot (\mathbf{x_{NDACC}} - \mathbf{x_{a,IASI}}) \tag{1}$$

where $\hat{\mathbf{x}}_{\mathbf{NDACC}}$ is the smoothed or convolved NDACC CH_4 profile and $\mathbf{x_{a,IASI}}$ and $\mathbf{A_{IASI}}$ are the IASI a priori profile and averaging kernel.

From the IASI and smoothed NDACC CH_4 profiles partial columns are calculated between 4 and 17 km. The average is taken of IASI pixels selected within 3 hours of the NDACC FTIR measurement, in a 0.5°-1.5° latitude-longitude-box centred around

5   the point on the line of sight (LOS) where the FTIR measurement has maximum sensitivity (typically at 5km alitude on the LOS).

Fig. 9 summarizes the results in a bar chart giving the relative difference between IASI and smoothed NDACC partial columns between 4 and 17 km at the different NDACC stations. The relative mean difference Δ=(IASI-NDACC)/NDACC and standard deviation of the difference (σ) in percentage is given for each station. Relative mean differences between IASI and NDACC

10   lie between -1.93 and 0.67% (of which 7 stations out of 10 less than ±1%) with exception of the Thule station, where IASI is biased high with respect to NDACC by 4.4%. The standard deviation of the difference lies in the range 1.91 to 3.99% for the 10 stations.

It is important to compare these results with the uncertainty budget of the IASI and the NDACC CH_4 partial columns. As given by Rodgers and Connor (2003) (equation 30), $\mathbf{S_\Delta}$, the covariance of the difference IASI-NDACC, can be calculated as:

15
$$\mathbf{S_\Delta} = (\mathbf{A_{IASI}} - \mathbf{A_{IASI}A_{NDACC}})\mathbf{S_{a,IASI}}(\mathbf{A_{IASI}} - \mathbf{A_{IASI}A_{NDACC}})^T$$
$$+ \mathbf{S_{IASI}}$$
$$+ \mathbf{A_{IASI}S_{NDACC}A_{IASI}}$$

The first term is the smoothing uncertainty of the comparison ensemble (the smoothed and a priori-corrected NDACC and IASI product) with $\mathbf{S_{a,IASI}}$ the IASI a priori uncertainty covariance matrix. $\mathbf{S_{IASI}}$ is the IASI retrieval uncertainty covariance exluding

20   the smoothing uncertainty and $\mathbf{S_{NDACC}}$ is the NDACC retrieval uncertainty covariance without the smoothing uncertainty. We compare the systematic and random uncertainty on the difference directly to the mean difference and standard deviation of the difference between IASI and NDACC. NDACC provides systematic and random uncertainty covariances for the different stations, with exception of Jungfraujoch. For IASI we set the random uncertainty $\mathbf{S_{a,IASI}^{rand}}$ equal to the IASI apriori uncertainty covariance matrix used in the IASI retrieval. We calculated a systematic component $\mathbf{S_{a,IASI}^{syst}}$ with a 2% standard deviation of the

25   a priori profile values. Separating the systematic and random component of $\mathbf{S_{IASI}}$ is less straightforward. Here we only consider the IASI measurement uncertainty as the random uncertainty and we do not consider the systematic component.

Table 2 lists the results of this analysis with the relative mean differences, the standard deviation of the differences and the mean values of the systematic and random uncertainties. We have a good agreement where the IASI-NDACC mean differences lie within the systematic uncertainty. Also for Thule the mean difference of 4.40% is within the systematic uncertainty of

30   5.14%. The standard deviation of the difference is close to the random uncertainty, but for certain stations slighlty larger. This discrepancy could be due to an additional error associated with the grid conversions or a geolocation error which are not taken into account (Calisesi et al., 2005; Vigouroux , 2009). Another reason could be the current underestimation of the random uncertainty of the NDACC CH_4 retrievals. They were found to be less than 1% for 6 out of the 10 NDACC stations. The ongoing work in the GAIA-CLIM project will harmonize the error characterization for all NDACC stations in the coming

period. This comparison stresses the importance of this harmonization work.

Scatter plots of collocated partial columns are presented in Fig. 10. We find very good correlations (R = 0.71-0.88) for the **high-latitude** stations Eureka, Thule and Kiruna. High correlations (R>0.9) are found as well for the **mid-latitude** stations Jungfraujoch and Zugspitze, while the mid-latitude stations Toronto performs poorer with a correlation of 0.44. The **tropical**

5   island stations Maido and Mauna Loa show poor correlations (R = 0.41-0.50) although biases are below 1% for these stations. The tropical island station Izaña however shows a high correlation of 0.90. For the most Southern station Wollongong (34°S) we find a good correlation of 0.77. The poorer correlations at the Mauna Loa, Maido and Toronto stations could be attributed to the lower CH_4 variability we see at these locations compared to the other stations. In addition, at Mauna Loa and Toronto, we see a few outliers which could explain the poorer linear regression fit at these stations.

10   These results demonstrate the ability of the IASI data to well capture the temporal variation of CH_4.

6   Discussion, conclusion and outlook

Although CH_4 is a more effective greenhouse gas than CO_2, it has a much shorter atmospheric lifetime than CO_2 that can remain in the atmosphere for hundreds or thousands of years. Therefore the mitigation of CH_4 emissions provides an opportunity for alleviating climate change in the short-term future (Kirschke et al., 2013). Global monitoring of CH_4 is essential to

15   study the evolution of atmospheric CH_4 and to help increase our knowledge on how the different sources and sinks influence its atmospheric abundance.

In this paper, we presented a new IASI CH_4 retrieval product developed at BIRA-IASB. Global distributions of CH_4 were derived from IASI radiances with the ASIMUT-ALVL software based on the OEM. A detailed description of the forward model, the retrieval strategy and the use of PCC L1C data was given. CH_4 concentrations retrieved from raw radiances and

20   PCC-reconstructed radiances showed an excellent correlation and negligible mean differences of < 0.026% (< 0.46 ppb).

We presented the latitudinal distribution of the DOFS for different seasons. We showed that, between 60°S and 70°N, the DOFS values range between 1 (0.9) and 1.8 (1.6) for daytime (nighttime) retrievals for NH summer. In NH winter values can become less than 1 for latitudes > 40°N. In tropical scenes DOFS values are typically around 1.4, with a good sensitivity in the mid to upper troposphere.

25   A quality assessment of the retrieved IASI CH_4 product was given by a detailed comparison with ground-based FTIR observations recorded at 10 NDACC stations. The BIRA-IASB product was compared to smoothed NDACC FTIR CH_4 partial columns between 4 and 17 km for the years 2011 to 2014. We found a very good agreement between both products with differences within the systematic uncertainty. Mean difference values range between -1.93 and 4.40% for the 10 stations. Absolute differences are less than 1% for 7 stations out of 10. The standard deviation of the difference lies in the range 1.91 to 3.99%

30   for all the stations. These values are close to the random uncertainty of IASI and NDACC, but for certain stations slightly larger. Possible reasons for this discrepancy could be an underestimation of the NDACC CH_4 random uncertainty or additional error sources not considered in the calculation of the random uncertainty, such as a regridding or geolocation error. Very good correlations are found for 7 out of the 10 NDACC stations with correlation coefficients between 0.71 and 0.96. Particularly for

Atmospheric
Measurement
Techniques
Discussions

the 3 high-latitude stations we find high correlations, as well as for the 2 high-quality mid-latitude stations Jungfraujoch and Zugspitze. With these results we are confident that the IASI data is capturing the mid to upper CH_4 variability well.

Future work will focus on extending the validation with additional datasets. Validation measurements for atmospheric vertical profiles for CH_4 are limited and very diverse. An innovative atmospheric sampling system called AirCore (Karion et al., 2010;

5 Membrive et al. , 2016) has been demonstrated to be a reliable concept to make vertical profile measurements of CO_2, CH_4 and CO from the surface up to ∼30 km. Although campaign-based, these high precision measurements provide a promising and novel validation tool. One of the next steps is to compare the IASI CH_4 with AirCore CH_4 profiles. Further, a global scale comparison with the neural network IASI-CH_4 product (Crevoisier et al., 2009) or with one of the new OEM IASI-CH_4 products recently published and under revision (Siddans et al., 2016; García et al., 2017) would be of particular interest.

10 IASI provides day- and nighttime measurements over land and sea and has a high spatial coverage. Its follow-up missions guarantee a long continuity of observations and its successor, the IASI-NG next-generation instrument, will ensure a continuity of data until after 2040. IASI-NG's spectral resolution and signal-to-noise ratio will be improved by a factor of two. It will fly on the three second-generation MetOp-SG-A series, scheduled to launch in 2021, 2028 and 2035. IASI provides therefore a great opportunity for continuous monitoring of the atmospheric composition on a fine spatio-temporal scale.

15 CH_4 is a challenging component to retrieve in the thermal infrared. Water vapour interferes strongly in the CH_4 thermal band. The same holds for the greenhouse gas N_2O which is strongly correlated to CH_4. In addition, spectroscopic uncertainties and mixing of spectral lines are still important issues in the CH_4 ν4 band. Continuous efforts will be made on improving the IASI CH_4 retrievals as to these issues and enhancing their precision. Furthermore, future work will focus on comparing the IASI concentrations with tagged simulations of CH_4 to see whether the model output is supported by the IASI data. With this re-

20 search we want to provide a better understanding of the CH_4 budget, which can help target the pertinent sources for reducing CH_4 emissions and the associated climate impact of this greenhouse gas.

The BIRA-IASB IASI CH_4 dataset is available through the European Space Agency (ESA) CCI-GHG project and can be downloaded from http://iasi.aeronomie.be/. Data is available for the years 2011-2014 between 60°S and 70°N and CH_4 profiles, a priori profiles, retrieval uncertainties and averaging kernels are provided.

Atmospheric
Measurement
Techniques
Discussions

References

Buchwitz, M., M. Reuter, O. Schneising, H. Boesch, I. Aben, M. Alexe, R. Armante, P. Bergamaschi, H. Bovensmann, D. Brunner, B. Buchmann, J. P. Burrows, A. Butz, F. Chevallier, A. Chedin, C. D. Crevoisier, M. De Maziere , E. De Wachter, R. Detmers, B. Dils, C. Frankenberg, S. Gonzi, P. Hahne, O. P. Hasekamp, W. Hewson, J. Heymann, S. Houweling, M. Hilker, T. Kaminski, G. Kuhlmann, A.

5   Laeng, T. T. v. Leeuwen, G. Lichtenberg, J. Marshall, S. Noel, J. Notholt, P. I. Palmer, R. Parker, P. Somkuti, M. Scholze, G. P. Stiller, T. Warneke, C. Zehner, THE GREENHOUSE GAS PROJECT OF ESA's CLIMATE CHANGE INITIATIVE (GHG-CCI): PHASE 2 ACHIEVEMENTS AND FUTURE PLANS, ESA ATMOS 2015 conference proceedings (ESA SP-735), Heraklion, Greece, 8-12 June 2015, 2015.

Calisesi, Y., V. T. Soebijanta, and R. van Oss (2005), Regridding of remote soundings: Formulation and application to ozone profile compar-
10   ison, J. Geophys. Res., 110, D23306, doi:10.1029/2005JD006122.

Clerbaux, C., Boynard, A., Clarisse, L., George, M., Hadji-Lazaro, J., Herbin, H., Hurtmans, D., Pommier, M., Razavi, A., Turquety, S., Wespes, C. and Coheur, P.-F.: Monitoring of atmospheric composition using the thermal infrared IASI/MetOp sounder, Atmos. Chem. Phys., 9, 6041-6054, 2009.

Clerbaux, C., Coheur, P.-F., Bauduin, S., Boynard; A., Clarisse, L., et al.. Doniki, S., George, M., Hadji-Lazaro, J., Hurtmans, D., Lacour,
15   J.-L., Ronsmans, G., Van Damme, M., Wespes, C. and Whitburn, S., Tracking pollutants from space: 10 years of IASI satellite observation, IGAC 2016 Science Conference (International Global Atmospheric Chemistry), Sep. 2016, Breckenridge, United States.

Crevoisier, C., Nobileau, D., Fiore, A. M., Armante, R., Chédin, A., and Scott, N. A.: Tropospheric methane in the tropics - first year from IASI hyperspectral infrared observations, Atmos. Chem. Phys., 9, 6337-6350, doi:10.5194/acp-9-6337-2009, 2009.

De Wachter, E., Barret, B., Le Flochmoën, E., Pavelin, E., Matricardi, M., Clerbaux, C., Hadji-Lazaro, J., George, M., Hurtmans, D., Coheur,
20   P.-F., Nedelec, P., and Cammas, J. P.: Retrieval of MetOp-A/IASI CO profiles and validation with MOZAIC data, Atmos. Meas. Tech., 5, 2843-2857, doi:10.5194/amt-5-2843-2012, 2012.

Dlugokencky, E.J., Houweling, S., Bruhwiler, L., Masarie, K.A., Lang, P.M., Miller, J.B. and Tans, P.P. 2003. Geophysical Research Letters 30: 10.1029/2003GL018126.

Dlugokencky, E. J.; Bruhwiler, L.; White, J. W. C.; Emmons, L. K.; Novelli, P. C.; Montzka, S. A.; Masarie, K. A.; Lang, P. M.; Crotwell, A.
25   M.; Miller, J. B. and Gatti, L. V., Observational constraints on recent increases in the atmospheric CH4 burden, Geophys. Res. Lett., 36, L18803, doi:10.1029/2009GL039780.

Vandaele, A.-C., Daerden, F., Fussen, D., Mahieux, A., Neary, L., Neefs, E., Robert, S., Willame, Y., Wilquet, V., Studying methane and other trace species in the Mars atmosphere using a SOIR instrumentOriginal Research Article, Planet. Space Sci. 59, 292-298.

Frankenberg, C., Meirink, J. F., Bergamaschi, P., Goede, A. P. H., Heimann, M., Körner, S., Platt, U., van Weele, M., and Wagner, T.: Satellite
30   chartography of atmospheric methane from SCIAMACHY on board ENVISAT: Analysis of the years 2003 and 2004, J. Geophys. Res., 111, D07303, doi:10.1029/2005JD006235, 2006.

García, O. E., Sepúlveda, E., Schneider, M., Wiegele, A., Borger, C., Hase, F., Barthlott, S., Blumenstock, T., and de Frutos, À. M.: Upper tropospheric CH4 and N2O retrievals from MetOp/IASI within the project MUSICA, Atmos. Meas. Tech. Discuss., doi:10.5194/amt-2016-326, in review, 2017.

35   Hu, H., Hasekamp, O., Butz, A., Galli, A., Landgraf, J., Aan de Brugh, J., Borsdorff, T., Scheepmaker, R., and Aben, I., The operational methane retrieval algorithm for TROPOMI, Atmos. Meas. Tech., 9, 5423-5440, doi:10.5194/amt-9-5423-2016, 2016.

Huijnen, V., Williams, J., van Weele, M., van Noije, T., Krol, M., Dentener, F., Segers, A., Houweling, S., Peters, W., de Laat, J., Boersma, F., Bergamaschi, P., van Velthoven, P., Le Sager, P., Eskes, H., Alkemade, F., Scheele, R., Nédélec, P., and Pätz, H.-W.: The global chemistry transport model TM5: description and evaluation of the tropospheric chemistry version 3.0, Geosci. Model Dev., 3, 445-473, doi:10.5194/gmd-3-445-2010, 2010.

5   Hultberg, T.: IASI Principal Component Compression (IASI PCC) FAQ and IASI Level 1 PCC Product Format Specification, Technical notes, available online at: http://www.eumetsat.int/website/home/Data/Products/Level1Data/index.html?lang=EN, 2009.

Jacob, D. J., Turner, A. J., Maasakkers, J. D., Sheng, J., Sun, K., Liu, X., Chance, K., Aben, I., McKeever, J., and Frankenberg, C.: Satellite observations of atmospheric methane and their value for quantifying methane emissions, Atmos. Chem. Phys., 16, 14371-14396, doi:10.5194/acp-16-14371-2016, 2016.

10   Jardine, C.N., Boardman, B., Osman, A., Vowles, J. and Palmer, J. (eds) Methane UK. Environmental Change Institute, University of Oxford, 64–71, http://www.eci.ox.ac.uk/research/energy/archive-methane.html

Karion, A., Sweeney, C., Tans, P., and Newberger, T.: AirCore: An Innovative Atmospheric Sampling System, Journal of Atmospheric and Oceanic Technology, 27, 1839–1853, doi:10.1175/2010JTECHA1448.1, http://www.esrl.noaa.gov/gmd/ccgg/aircore/, 2010.

Kirschke, S., Bousquet, P., Ciais, P., Saunois, M., Canadell, J. G., Dlugokencky, E. J., Bergamaschi, P., Bergmann, D., Blake, D. R., Bruhwiler,
15   L., Cameron-Smith, P., Castaldi, S., Chevallier, F., Feng, L., Fraser, A., Heimann, M., Hodson, E. L., Houweling, S., Josse, B., Fraser, P. J., Krummel, P. B., Lamarque, J.-F., Langenfelds, R. L., Le Quere, C., Naik, V., O'Doherty, S., Palmer, P. I., Pison, I., Plummer, D., Poulter, B., Prinn, R. G., Rigby, M., Ringeval, B., Santini, M., Schmidt, M., Shindell, D. T., Simpson, I. J., Spahni, R., Steele, L. P., Strode, S. A., Sudo, K., Szopa, S., Van Der Werf, G. R., Voulgarakis, A., Van Weele, M., Weiss, R. F., Williams, J. E. and Zeng, G. Three decades of global methane sources and sinks Nature Geoscience, Nature Publishing Group, 2013, 6, 813-823.

20   Krol, M., Houweling, S., Bregman, B., van den Broek, M., Segers, A., van Velthoven, P., Peters, W., Dentener, F., and Bergamaschi, P.: The two-way nested global chemistry-transport zoom model TM5: algorithm and applications, Atmos. Chem. Phys., 5, 417-432, doi:10.5194/acp-5-417-2005, 2005.

Kuze, A., Suto, H., Shiomi, K., Kawakami, S., Tanaka, M., Ueda, Y., Deguchi, A., Yoshida, J., Yamamoto, Y., Kataoka, F., Taylor, T. E., and Buijs, H. L.: Update on GOSAT TANSO-FTS performance, operations, and data products after more than 6 years in space, Atmos. Meas.
25   Tech., 9, 2445–2461, doi:10.5194/amt-9-2445-2016, 2016.

Membrive, O., Crevoisier, C., Sweeney, C., Danis, F., Hertzog, A., Engel, A., Bönisch, H., and Picon, L.: AirCore-HR: A high resolution column sampling to enhance the vertical description of CH4 and CO2, Atmos. Meas. Tech. Discuss., doi:10.5194/amt-2016-236, in review, 2016.

Mishchenko, M.I., Travis, L.D., 1998. Capabilities and limitations of a current Fortran implementation of the T-matrix method for randomly
30   oriented, rotationally symmetric scatterers. J. Quant. Spectrosc. Radiat. Transf. 60 (3), 309-324.

Myhre, G., D. Shindell, F.-M. Bréon, W. Collins, J. Fuglestvedt, J. Huang, D. Koch, J.-F. Lamarque, D. Lee, B. Mendoza, T. Nakajima, A. Robock, G. Stephens, T. Takemura and H. Zhang, 2013: Anthropogenic and Natural Radiative Forc- ing. In: Climate Change 2013: The Physical Science Basis. Contribution of Working Group I to the Fifth Assessment Report of the Intergovernmental Panel on Climate Change [Stocker, T.F., D. Qin, G.-K. Plattner, M. Tignor, S.K. Allen, J. Boschung, A. Nauels, Y. Xia, V. Bex and P.M. Midgley (eds.)].
35   Cambridge University Press, Cambridge, United Kingdom and New York, NY, USA.

Nisbet, E. G., E. J. Dlugokencky, and P. Bousquet (2014), Methane on the rise - Again, Science, 343, 493–5.

Patra, P. K., X. Xiong, C. Barnet, E. J. Dlugokencky, U. Karin, K. Tsuboi, and D. Worthy, Validation of CH4 surface emission using forward chemistry-transport model, Baltimore, April 2009.

Atmospheric
Measurement
Techniques
Open Access
Discussions
EGU

C. Pierangelo, B. Millet, F. Esteve, M. Alpers, G. Ehret, P. Flamant, S. Berthier, F. Gibert, O. Chomette, D. Edouart, C. Deniel, P. Bousquet and F. Chevallier, MERLIN (Methane Remote Sensing Lidar Mission): an Overview, EPJ Web of Conferences 119 26001 (2016), DOI: 10.1051/epjconf/201611926001

Razavi, A., Clerbaux, C., Wespes, C., Clarisse, L., Hurtmans, D., Payan, S., Camy-Peyret, C., and Coheur, P. F.: Characterization of methane
5   retrievals from the IASI space-borne sounder, Atmos. Chem. Phys., 9, 7889-7899, doi:10.5194/acp-9-7889-2009, 2009.

Robert, S., Vandaele, A.C. , Thomas, I. , Willame, Y., Daerden, F., Delanoye, S., Depiesse, C., Drummond, R., Neefs, E., Neary, L., Ristic, B., Mason, J., Lopez-Moreno, J.-J., Rodriguez-Gomez, J., Patel, M.R., Bellucci, G., The NOMAD Team., Expected performances of the NOMAD/ExoMars instrument. Planetary and Space Science (2016), http://dx.doi.org/10.1016/j.pss.2016.03.003.

Rodgers, C.D.: Inverse methods for atmospheric sounding: Theory and Practice. Singapore: World Scientific Publishing Co. Pte. Ltd., 2000.
10 Rodgers, C.D. and Connor, B.J.: Intercomparison of remote sounding instruments, J. Geophys. Res., 108, 4116-4129, 2003.

Rothman, L., Gordon, I., Babikov, Y., Barbe, A., Benner, D. C., Bernath, P., Birk, M., Bizzocchi, L., Boudon, V., Brown, L., Campargue, A., Chance, K., Cohen, E., Coudert, L., Devi, V., Drouin, B., Fayt, A., Flaud, J.-M., Gamache, R., Harrison, J., Hartmann, J.-M., Hill, C., Hodges, J., Jacquemart, D., Jolly, A., Lamouroux, J., Roy, R. L., Li, G., Long, D., Lyulin, O., Mackie, C., Massie, S., Mikhailenko, S., Müller, H., Naumenko, O., Nikitin, A., Orphal, J., Perevalov, V., Perrin, A., Polovtseva, E., Richard, C., Smith, M., Starikova, E., Sung,
15 K., Tashkun, S., Tennyson, J., Toon, G., Tyuterev, V. and Wagner, G., The HITRAN2012 molecular spectroscopic database Journal of Quantitative Spectroscopy and Radiative Transfer , 2013, 130, 4-50.

Siddans, R., Knappett, D., Waterfall, A., Hurley, J., Latter, B., Kerridge, B., Boesch, H., and Parker, R.: Global height-resolved methane retrievals from the Infrared Atmospheric Sounding Interferometer (IASI) on MetOp, Atmos. Meas. Tech. Discuss., doi:10.5194/amt-2016-290, in review, 2016.

20 Vandaele, A.C., Kruglanski, M., De Mazière, M., Modelling and retrieval of Atmospheric spectra using ASIMUT in Proc. of the First 'Atmospheric Science Conference', ESRIN, Frascati, Italy, 8 – 12 May 2006.

Vandaele, A.C.,De Mazière, M., Drummond, R., Mahieux, A., Neefs, E., Wilquet, V., Korablev, O., Fedorova, A., Belyaev., D., Montmessin, F., Bertaux, J.-L., 2008. Composition of the Venus mesosphere measured by SOIR on board Venus Express. J. Geophys. Res. 113. http://dx.doi.org/10.1029/2008JE003140.

25 Vandenbussche, S., Kochenova, S., Vandaele, A. C. , Kumps, N. , De Mazière, M., Retrieval Of Desert Dust Aerosol Vertical Profiles From Iasi Measurements In The Tir Atmospheric Window, Atmos. Meas. Tech. 6, 2577-2591, 2013.

van Weele, M., Williams, J. E., van Velthoven, P. F.J. , Schuck, T. J., Brenninkmeijer, C. A.M., Methane variability in the upper troposphere and lower stratosphere and their relevance for emission inversions constrained by satellite observations, Conference Proceedings Non CO2 Greenhouse Gases, Amsterdam, Volume: 6, November 2011.

30 Worden, J., Kulawik, S., Frankenberg, C., Payne, V., Bowman, K., Cady-Peirara, K., Wecht, K., Lee, J.-E., and Noone, D.: Profiles of CH4, HDO, H2O and N2O wuth improved tropospheric vertical resolution from Aura TES radiances, Atmos. Meas. Tech., 5, 397-411, doi:10.5194/amt-5-397-2012, 2012.

Saunois, M., Jackson, R. B., Bousquet, P., Poulter, B. and Canadell, J. G. The growing role of methane in anthropogenic climate change Environmental Research Letters, 2016, 11, 120207.

35 Shindell, D., J.C.I. Kuylenstierna, E. Vignati, R. van Dingenen, M. Amann, Z. Klimont, S.C. Anenberg, N. Muller, G. Janssens-Maenhout, F. Raes, J. Schwartz, G. Faluvegi, L. Pozzoli, K. Kupiainen, L. Höglund-Isaksson, L. Emberson, D. Streets, V. Ramanathan, K. Hicks, N.T.K. Oanh, G. Milly, M. Williams, V. Demkine, and D. Fowler, 2012: Simultaneously mitigating near-term climate change and improving human health and food security. Science, 335, 183-189, doi:10.1126/science.1210026.

Atmospheric
Measurement
Techniques
Discussions

Spurr, R.J.D., 2006. VLIDORT: a linearized pseudo-spherical vector discrete ordinate radiative transfer code for forward model and retrieval studies in multilayer multiple scattering media. J. Quant. Spectrosc. Radiat. Transf. 102, 316-342.

Vigouroux, C., Hendrick, F., Stavrakou, T., Dils, B., De Smedt, I., Hermans, C., Merlaud, A., Scolas, F., Senten, C., Vanhaelewyn, G., Fally, S., Carleer, M., Metzger, J.-M., Müller, J.-F., Van Roozendael, M., and De Mazière, M.: Ground-based FTIR and MAX-DOAS
5   observations of formaldehyde at Réunion Island and comparisons with satellite and model data, Atmos. Chem. Phys., 9, 9523-9544, doi:10.5194/acp-9-9523-2009, 2009.

http://www.wmo.int/pages/prog/arep/gaw/ghg/GHGbulletin.html

Xiong, X., Barnet, C., Maddy, E., Sweeney, C., Liu, X., Zhou, L., and Goldberg, M.: Characterization and validation of methane products from the Atmospheric Infrared Sounder (AIRS), J. Geophys. Res., 113, G00A01, doi:10.1029/2007JG000500, 2008.

10 Xiong, X., C. D. Barnet, Q. Zhuang, T. Machida, C. Sweeney, and P. K. Patra (2010), Mid-upper tropospheric methane in the high Northern Hemisphere: Spaceborne observations by AIRS, aircraft measurements, and model simulations, J. Geophys. Res., 115, D19309, doi:10.1029/2009JD013796.

Xiong, X., Barnet, C., Maddy, E. S., Gambacorta, A., King, T. S., and Wofsy, S. C.: Mid-upper tropospheric methane retrieval from IASI and its validation, Atmos. Meas. Tech., 6, 2255–2265, doi:10.5194/amt-6-2255-2013, 2013.

15 Zhou, D.K., Larar, A.M., Liu, X., Smith, W.L., Strow, L.L. and Yang, P.: Global Land Surface Emissivity Retrieved From Satellite Ultra-spectral IR Measurements, IEEE Trans. Geosci. Remote. Sens., 49(4), 1277?1290, doi:10.1109/TGRS.2010.2051036, 2011.
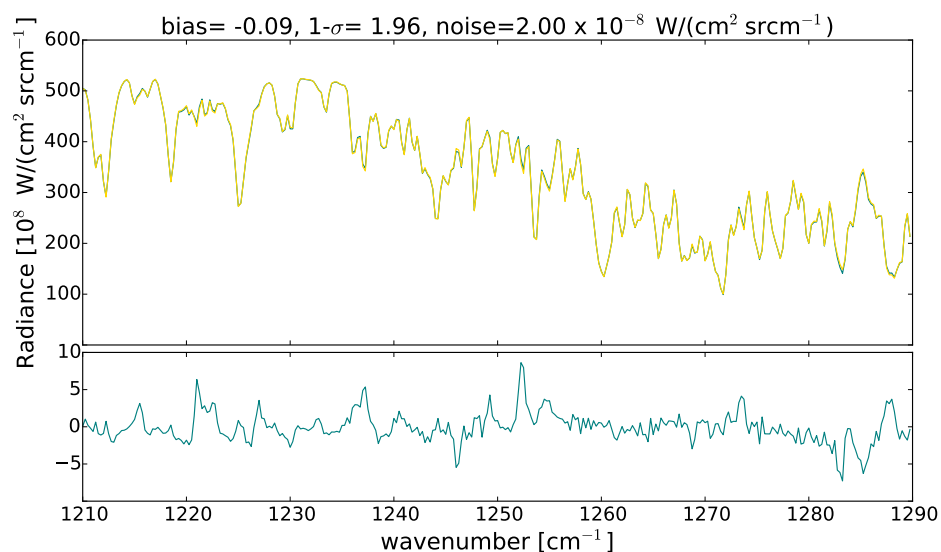
Figure 1. [top] Measured (blue) and simulated (yellow) radiances. [bottom] Measured minus simulated radiances. The mean difference (bias), 1-σ standard deviation of the difference and radiometric noise-value used in the retrieval (all in x 10^{-8} W/(m^2 sr m^{-1})) are given in the title.
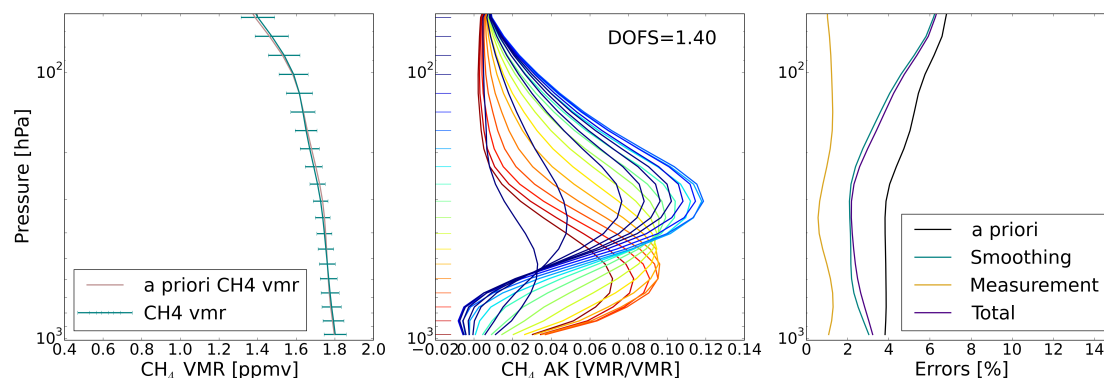
Figure 2. [left] Retrieved and a priori CH_4 vmr profile in ppmv for an observation on the 2nd of July 2013. [middle] Averaging kernel of the retrieval with a DOFS of 1.40. [right] CH_4 uncertainty profiles in percentage. Given are the measurement (yellow) and smoothing (blue) uncertainty which contribute to the total (purple) uncertainty. The black line represents the variability of the a priori as calculated from the square root of the diagonal elements of the a priori uncertainty covariance matrix S_a.

Atmospheric
Measurement
Techniques
Open Access
Discussions

EGU

	CH$_4$
Spectral range	1210-1290 cm^{-1}
State vector	CH$_4$, H$_2$O and N$_2$O profile,
	CO$_2$ total column, T$_{skin}$
Pressure, temperature, RH	IASI L2
Spectroscopy	HITRAN 2012
Emissivity	Zhou et al. (2011)
a priori information	WACCM

**Table 1.** Characteristics BIRA-IASB CH$_4$ retrieval.
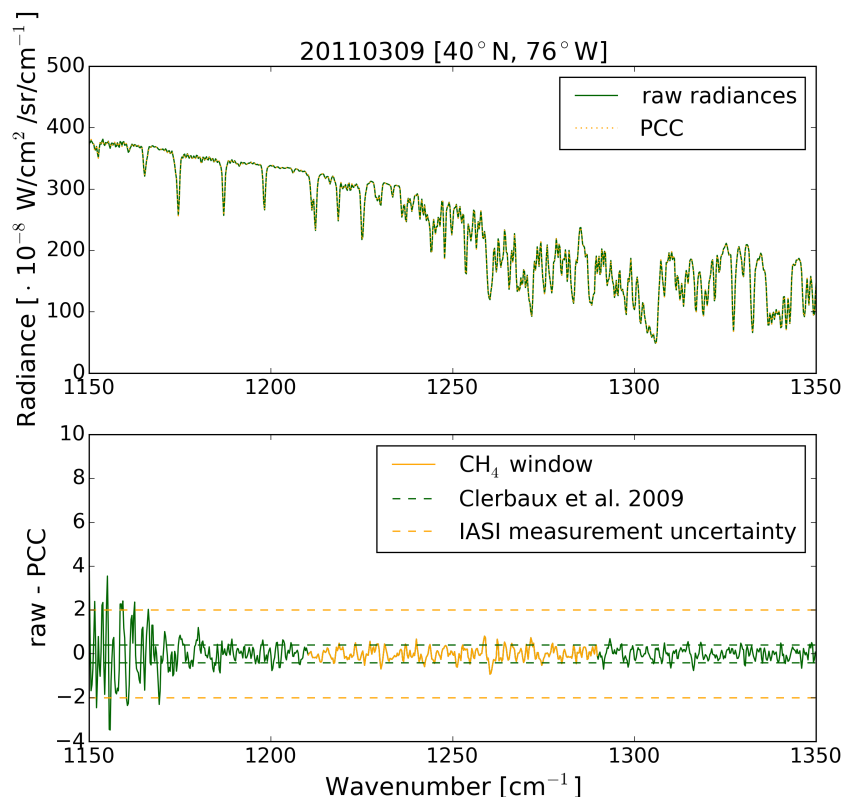
Figure 3. Radiances from a nighttime pixel on the 9th of March 2011 at 40°N and 76°W. [top] Raw radiances and PCC-reconstructed radiances. [bottom] Difference between raw radiances and PCC radiances. The CH_4 spectral retrieval window is highlighted in orange. The green horizontal dashed lines indicates the IASI radiometric noise at $1250 \, \text{cm}^{-1}$ as given by Clerbaux et al. (2009) and the orange horizontal dashed lines indicate the IASI radiometric noise defined in the retrieval (see Sect. 3.1). The differences between the raw and PCC radiances are within the IASI radiometric noise.
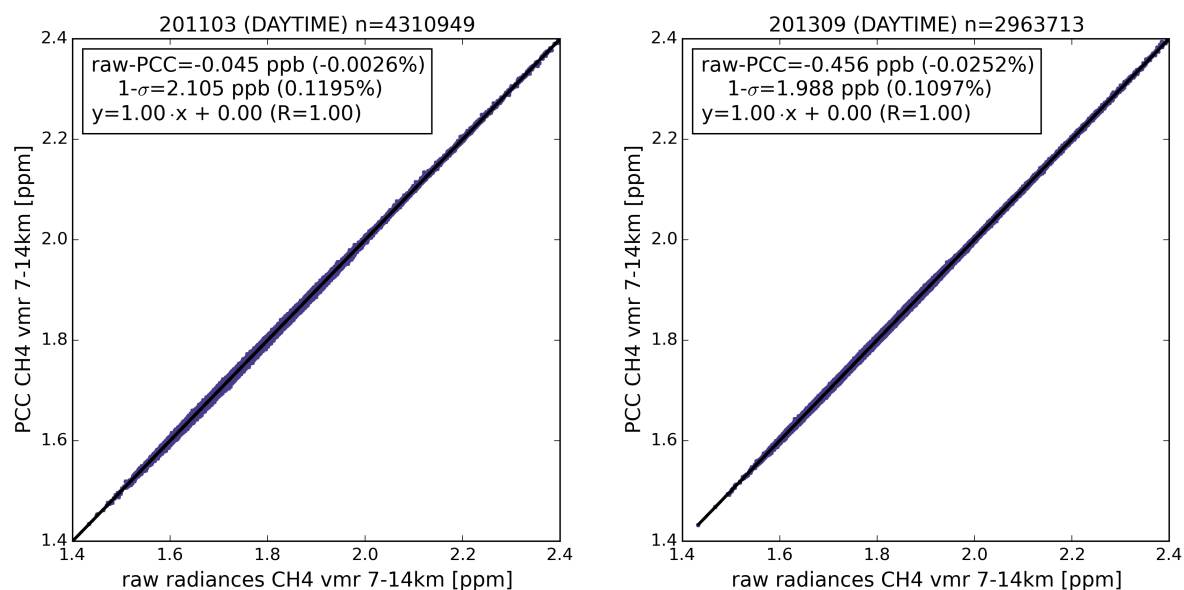
Figure 4. Correlation plot retrieved CH$_4$ between 7 and 14 km from the raw radiances (x-axis) and from the PCC-reconstructed radiances (y-axis) for March 2011 [left] and September 2013 [right], for daytime retrievals between 60°S and 70°N. The mean difference and 1-σ of the difference between raw and PCC partial columns is given in ppb and % in the legend, as well as the slope and intercept from the least-squares fit and correlation coefficient R.
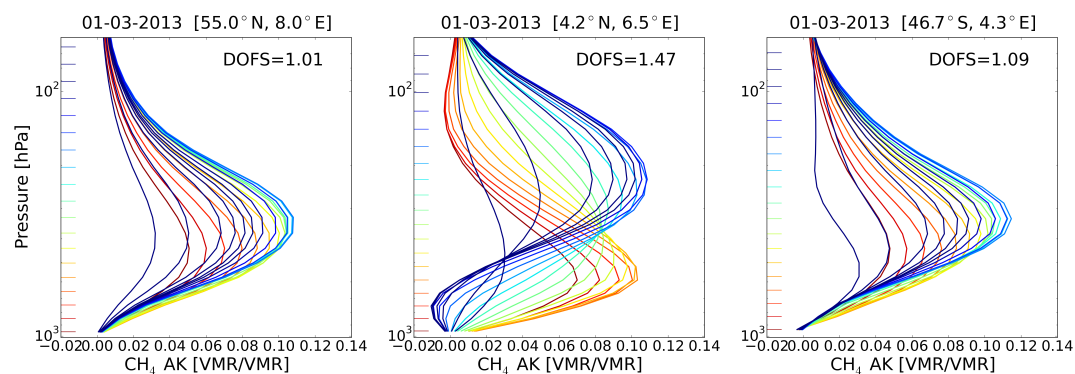
Figure 5. CH$_4$ averaging kernels for 3 pixels on the 1st of March 2013 at 3 different locations (55°N, 4°N and 47°S).

Atmospheric
Measurement
Techniques
Open Access

Discussions

EGU
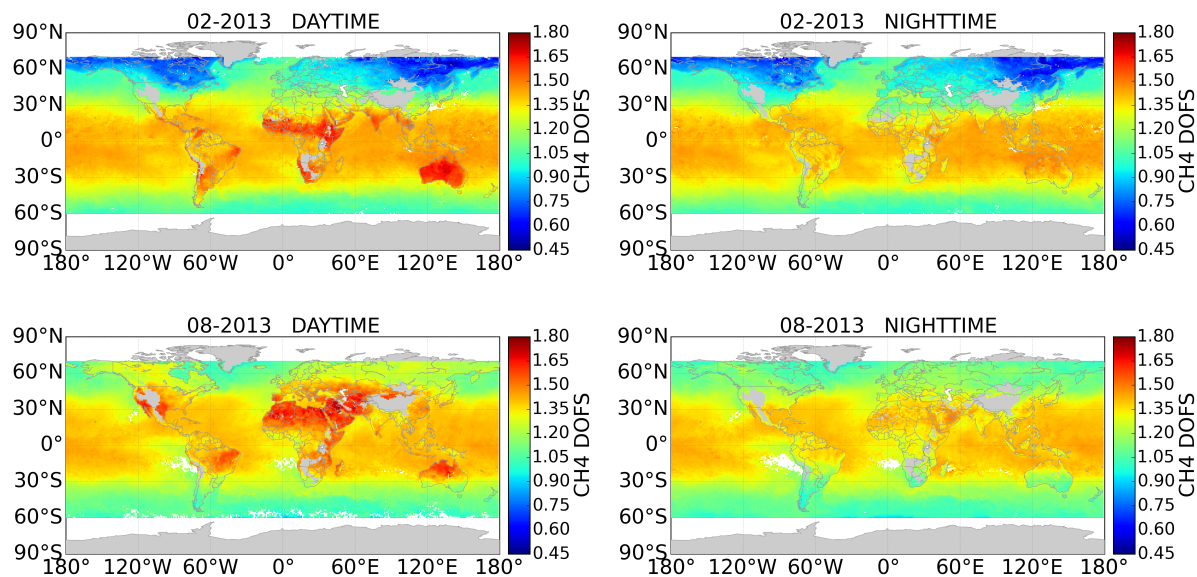
Figure 6. Maps of the CH_4 Degrees of Freedom for signal (DOFS) calculated from the trace of the CH_4 averaging kernel, for February [top] and August [bottom] 2013. DOFS for daytime observations are given on the left, DOFS for nighttime observations on the right.

Atmospheric
Measurement
Techniques

Open Access

Discussions

EGU
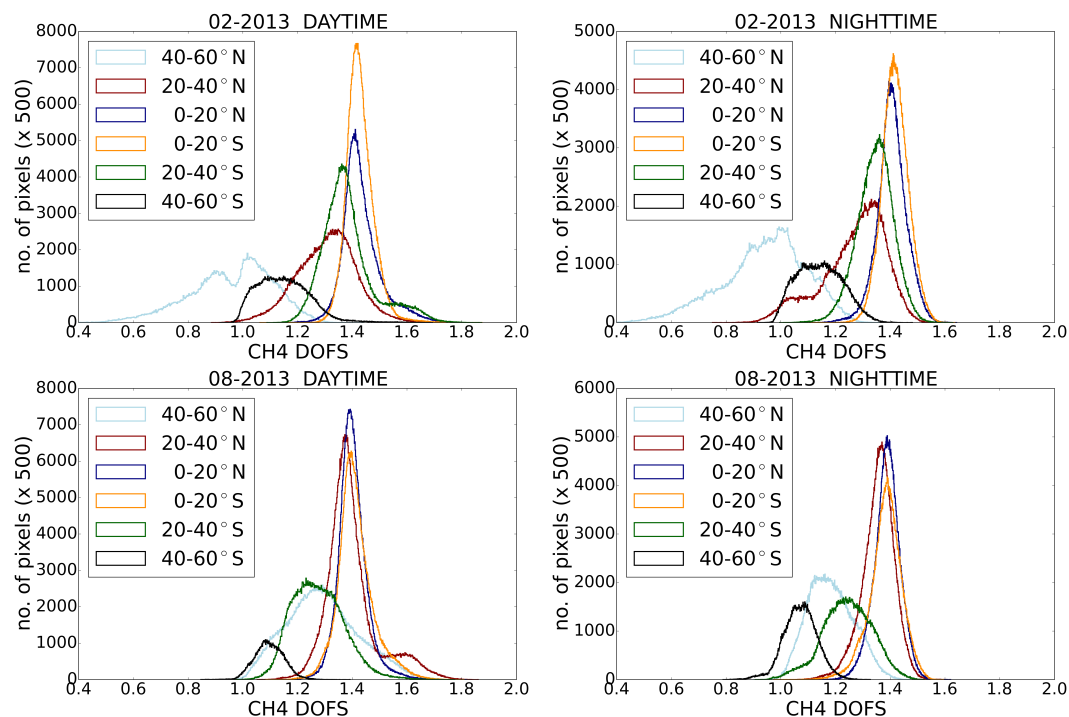
Figure 7. CH$_4$ DOFS for different latitudinal bands for daytime [left] and nighttime [right] observations for February [top] and August [bottom] 2013.

| site	LAT	$\Delta[\%]$	σ [%]	ϵ_{sys} [%]	ϵ_{rand} [%]	R	n
Eureka	80°N	-0.51	3.99	7.33	1.98	**0.71**	501
Thule	77°N	4.40	3.65	5.25	2.24	**0.84**	244
Kiruna	68°N	0.26	2.20	3.62	2.52	**0.88**	445
Jungfraujoch	47°N	-0.58	2.23	NA	NA	**0.96**	737
Zugspitze	47°N	-0.13	2.56	2.24	2.33	**0.92**	2123
Toronto	44°N	-1.93	3.57	8.32	3.15	0.44	612
Izana	28°N	-1.38	1.91	3.32	2.28	**0.90**	3931
Mauna Loa	20°N	0.67	3.27	4.81	2.44	0.41	734
Maido	21°S	0.25	3.14	3.49	2.90	0.50	547
Wollongong	34°S	-0.47	2.24	6.70	6.20	**0.77**	2293

Table 2. Statistics of the comparison between the IASI and smoothed NDACC CH$_4$ 4-17 km partial columns for the period 2011-2014. For each location, the latitude coordinates, the mean percentage difference (Δ=(IASI-NDACC)/NDACC) and standard deviation of the difference (σ), the mean systematic (ϵ_{sys}) and random uncertainty of the differences (ϵ_{rand}), the correlation coefficient (R) and the number of observations (n) are given. NA=not available, for Jungfraujoch the systematic and random uncertainty covariance matrices are not available.
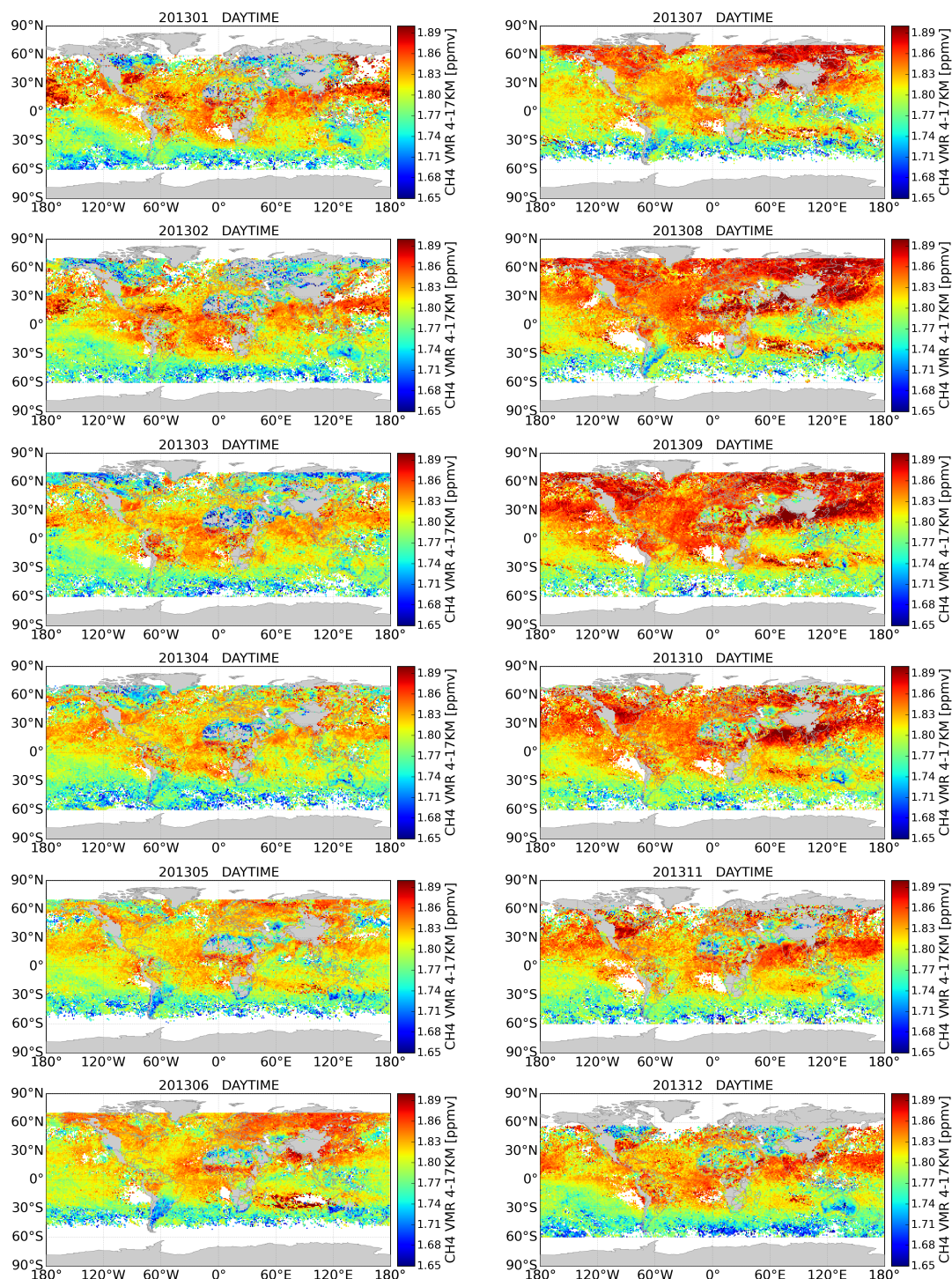
Figure 8. Monthly mean global daytime distributions of CH_4 partial columns (4-17 km) in 2013. Given is the average over the 2 x 2 circular pixels which are measured simultaneously by IASI. The pixels are binned on a 1° x 1° grid.

Atmospheric
Measurement
Techniques
Discussions
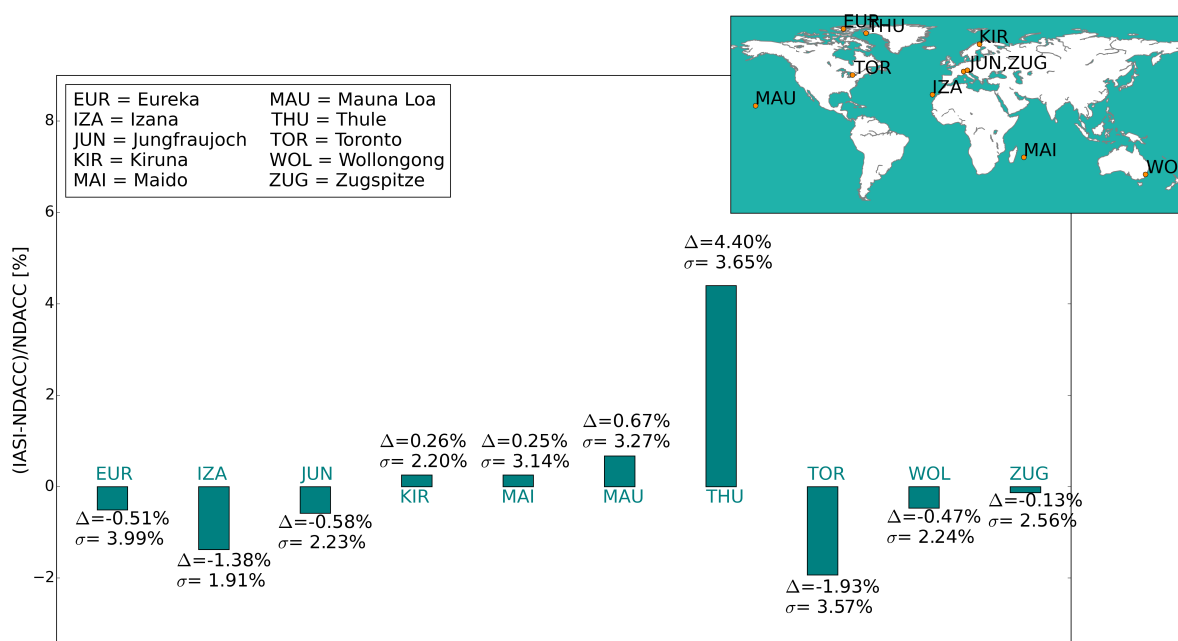
Figure 9. Barchart of the results of the IASI-NDACC validation exercise. Given is the relative percentage difference Δ=(IASI-NDACC)/NDACC and standard deviation of the difference (σ) of partial columns in the 4-17 km altitude range for each of the 10 investigated NDACC sites, visualized in the map on the top right. These results are also summarized in Table 2.
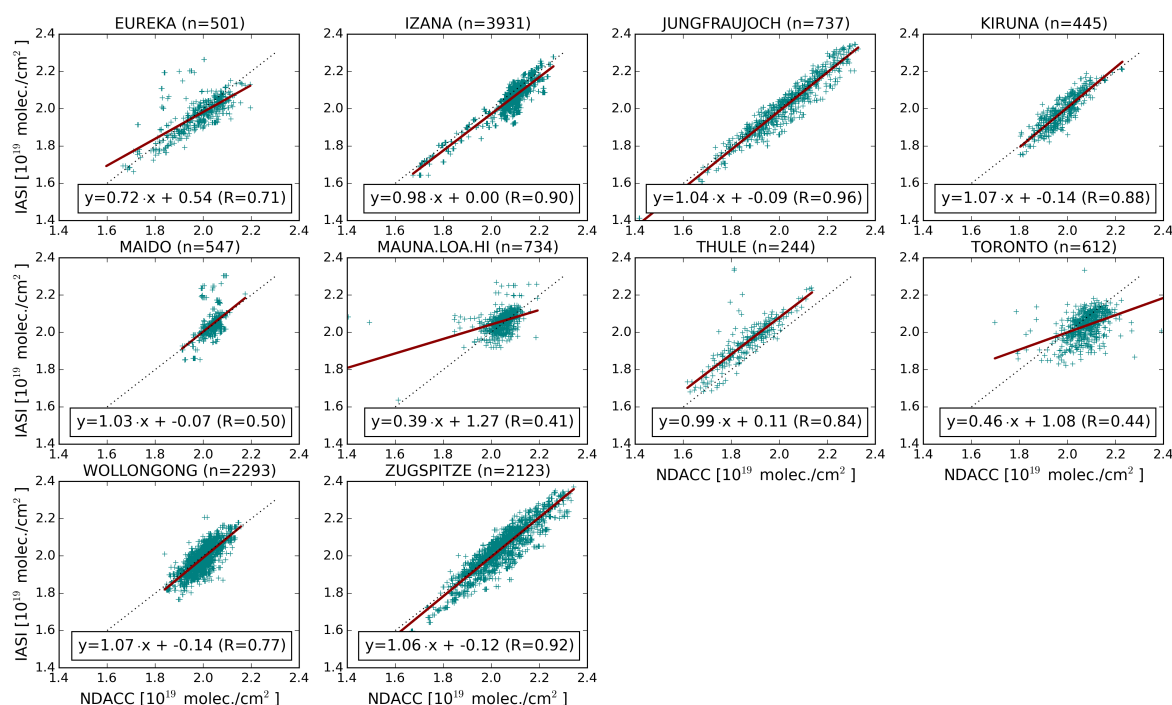
Figure 10. Correlation plots of smoothed NDACC and IASI CH_4 partial columns (4-17 km) in molec./cm^2 for the period 2011-2014. The number of collocations (n) is given for each site in the title. The red lines are the linear regressions between the data points and the dashed black line is the unity slope, shown for comparison. The values of the linear regression and the correlation coefficient (R) are given for each station, the latter is summarized in Table 2.